ELSEVIER

Investigation and modification of molecular structures with the nanoManipulator

M. Guthold,*†‡ M. Falvo,† W.G. Matthews,† S. Paulson,† J. Mullin,‡§ S. Lord,§ D. Erie,‡ S. Washburn,†§ R. Superfine,† F.P. Brooks Jr.,* and R.M. Taylor II*

**Computer Science Department, †Department of Physics and Astronomy, ‡Department of Chemistry, and §Department of Pathology, University of North Carolina, Chapel Hill, North Carolina, USA*

The nanoManipulator system adds a virtual reality interface to an atomic force microscope (AFM), thus providing a tool that enables the user not only to image but also to manipulate nanometer-sized molecular structures. As the AFM tip scans the surface of these structures, the tip–sample interaction forces are monitored, which in turn provide information about the frictional, mechanical, and topological properties of the sample. Computer graphics are used to reconstruct the surface for the user, with color or contours overlaid to indicate additional data sets. Moreover, by means of a force-feedback pen, which is connected to the scanning tip via software, the user can touch the surface under investigation to feel it and to manipulate objects on it. This system has been used to investigate carbon nanotubes, fibrin, DNA, adenovirus, and tobacco mosaic virus. Nanotubes have been bent, translated, and rotated to understand their mechanical properties and to investigate friction on the molecular level. AFM lithography is being combined with the nanoManipulator to investigate the electromechanical properties of carbon nanotubes. The rupture forces of fibrin and DNA have been measured. This article discusses how some of the graphics and interface features of the nanoManipulator made these novel investigations possible. Visitors have used the system to examine chromosomes, bacterial pili fibers, and nanochain aggregates (NCAs). Investigators are invited to apply to use the system as described on the web at http://www.cs.unc.edu/Research/nano/doc/biovisit.html. © *2000 by Elsevier Science Inc.*

Keywords: nanoManipulator, atomic force microscope, haptic, computer graphics, carbon nanotubes, friction, mechanical properties, rupture, fibrin, DNA, adenovirus, tobacco mosaic virus

Corresponding author: R.M. Taylor II, Computer Science Department, University of North Carolina at Chapel Hill, CB #3175, Sitterson Hall, Chapel Hill, NC 27599-3175, USA. Tel.: 919-962-1701; fax: 919-962-1799.

E-mail address: taylorr@cs.unc.edu (R.M. Taylor)

INTRODUCTION

This article reports on the nanoManipulator system (Figure 1a), which is one part of a long-running research program in molecular graphics at the University of North Carolina at Chapel Hill. Run by Frederick P. Brooks, Jr., this program has been funded as an NIH National Research Resource and has been serving biochemists since 1971. The nanoManipulator system couples scientists to real (as opposed to simulated) molecules through the use of an atomic force microscope (AFM). Thus, the first part of this article briefly describes the atomic force microscope. The second part treats the nanoManipulator system and examines the usefulness of the virtual reality and haptic (relating to or based on the sense of touch) feedback components of this system. The last part gives an overview of the latest scientific experiments that have been carried out with this system.

ATOMIC FORCE MICROSCOPY

In the 1980s a new generation of microscopes, the scanning probe microscopes (SPMs), was developed. Common to all these microscopes is that a probe is scanned over the sample while the probe–sample interactions are monitored. A host of information about many different samples has been obtained by using a large variety of scanning probes. Here, a particular type of scanning probe microscope, the atomic force microscope (AFM), is described briefly, as it is an integral part of the nanoManipulator. In an AFM, also known as a scanning force microscope (SFM),[1] the sample is scanned by a sharp tip, which is mounted on a flexible cantilever (Figure 1b). As the tip scans over the sample, the cantilever is deflected by the topographical features of the sample. These deflections are

Journal of Molecular Graphics and Modelling 17, 187–197, 1999

655 Avenue of the Americas, New York, NY 10010

1093-3263/99/$–see front matter
PII S1093-3263(99)00030-3

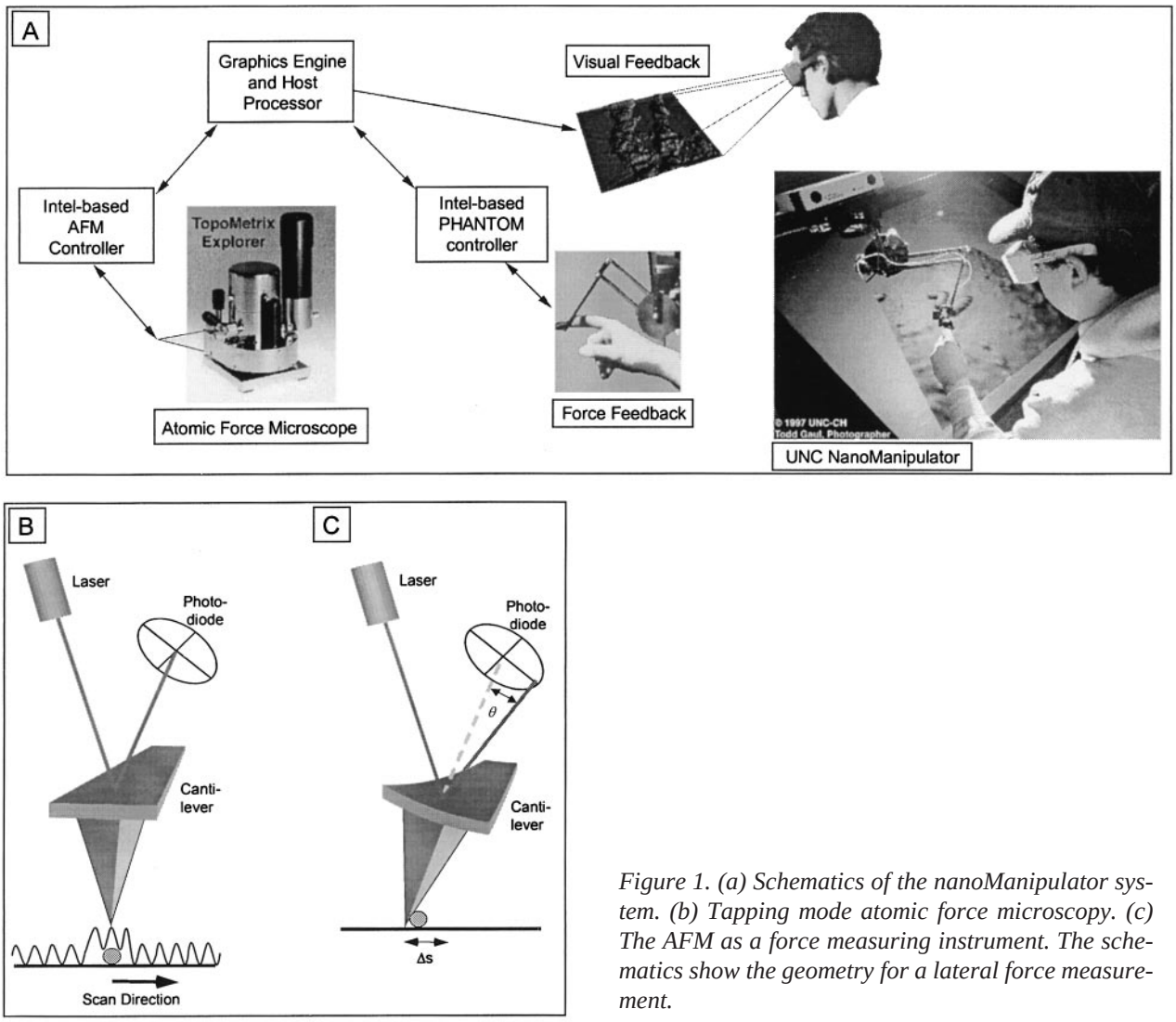

Figure 1. (a) Schematics of the nanoManipulator system. (b) Tapping mode atomic force microscopy. (c) The AFM as a force measuring instrument. The schematics show the geometry for a lateral force measurement.

usually recorded by an optical lever system. Frequently, the microscope is operated in the "constant force mode" or "constant amplitude mode" in which the normal force exerted on the sample by the tip is maintained at a set value. This is accomplished by a feedback loop that drives the sample up or down to counter changes in the lever deflection.

Tapping Mode versus Contact Mode Imaging

When a sample is scanned in *contact* mode AFM, the tip is in continuous contact with the sample and, therefore, significant normal and lateral forces may be exerted on the sample. For loosely attached samples, imaging in contact mode is sometimes difficult because the tip drags the sample along with it.[2] This problem has been overcome by the development of a new imaging mode, the *tapping* or *intermittent contact* mode (Figure 1b).[3] In this mode, the cantilever is oscillated perpendicular to the surface as it is scanned over the surface and the amplitude of the oscillation is used as the feedback signal. Hence, the tip touches the sample only intermittently, and lateral forces are nearly eliminated. The nanoManipulator exploits the difference between contact mode and tapping mode: Samples can be manipulated in contact mode while they can be imaged before and after a manipulation in tapping mode without further manipulating or damaging them.

One of the principal advantages of the SFM over other high-resolution microscopes is its ability to image in liquids[4] as well as in air. However, when using tapping mode in liquid, the common technique of driving the fluid chamber to excite the tip is confounded by the resonances of the chamber being indistinguishable from the resonance of the cantilever. A method to overcome this problem and to make imaging in liquids a more robust technique is to drive the cantilever directly.[5–7] For some of the experiments described in this article a *magnetic tapping* mode was used for imaging. A magnetic particle was glued to the back of the cantilever and an external, oscillating magnetic force was used to drive the cantilever for imaging in liquid. Using this technique high-resolution images of adenoviruses and DNA have been obtained.[8]

The AFM as a Force-Measuring Instrument

The AFM is an instrument that is used not only for imaging but, more and more, also for extremely sensitive force measurements. Depending on the cantilever, forces ranging from a

few piconewtons (in some cases attonewtons[9]) to several micronewtons can be measured—a range that is not accessible by any other single technique. The cantilever can be considered as an elastic spring and the force exerted on the sample is simply given by $F = -k \cdot \Delta s$, where k is the spring constant and Δs is the deflection of the lever. Forces can be measured in the normal and the lateral direction; Figure 1c depicts the geometry for lateral force measurements as the torsion of the cantilever is detected. The normal and lateral force constants of beamlike cantilevers can be calculated from $k_n = (Ewt^3)/(4L^3)$ and $k_t = (Gwt^3)/(3Ll_t^2)$,[10] where E and G are the Young's and shear modulus of the material, respectively; L, w, and t are the length, width, and thickness of the cantilever; and l_t is the length of tip. The absolute error in these force measurements is dominated by the error in determining the spring constant of the cantilever, and can be on the order of 30%. However, the relative errors within any given experiment are much smaller ($<1\%$).

Typically force measurements in the normal direction are more sensitive since the normal force constant is usually smaller than the lateral force constant. However, lateral force measurements have the advantage that the sample can be imaged before and after the manipulation. This is not always possible in normal force measurements, especially when the sample molecule is spanned between the tip and the substrate.

THE NANOMANIPULATOR

The nanoManipulator (Figure 1a) is an advanced graphics interface for an SPM, which allows scientists from a variety of disciplines to examine and manipulate nanometer-scale structures. As experiments are done, the data collected by the microscope are rendered in real time as a three-dimensional, directionally illuminated image, which makes the interpretation of height data more intuitive than in a simple two-dimensional display. The data are also used to provide information to a haptic (relating to or based on the sense of touch) interface that allows the user to "feel" the surface topography by directly controlling the tip. This is accomplished by relaying the data to an Intel-based PHANTOM controller (SensAble Technologies, Cambridge, MA). This feature allows the user to know the precise location of the tip, despite hysteresis in the sample-positioning mechanism, through the sense of touch. Most importantly, in addition to providing topographic information to the user, the hand-held stylus of the haptic device can also be used to perform controlled manipulations of the sample with the tip. The path chosen by the operator's hand as it moves the stylus is scaled down by a factor of about 10^7 (depending on the scan size) and is relayed to the tip. The difference in the lateral forces exerted by the tip on the sample when using contact mode or tapping mode is exploited when doing manipulations. The imaging method can be changed at will from tapping to contact. By controlling the force applied to the surface in contact mode and by positioning the tip carefully, lateral forces can be applied to modify a chosen object in a controlled manner. The nanoManipulator makes these manipulations straightforward, with a natural and transparent interface for the user. Before and after a manipulation the sample is imaged in tapping mode without further manipulating the sample. Studies have shown that the nanoManipulator greatly increases productivity by acting as a translator between the scientist and the instrument being controlled.[11] For more detailed information on this instrument, see Finch et al.[11] and Taylor et al.[12] or the web site http://www.cs.unc.edu/Research/nano.

Features of the NanoManipulator: Virtual Reality and Haptic Feedback

VR display The nanoManipulator provides a virtual reality interface to an AFM. This interface is compelling and engaging, as it allows the scientist to virtually see and touch nanometer-scale objects. However, the test of a scientific instrument is not how compelling it is but how *useful* it is. Tools are useful to science if they help produce new insight into problems of interest to the scientist. This section presents the scientific insights gained using the graphics and haptics portions of the interface. An additional treatment of the system capabilities and some of the resulting insights can be found in Taylor et al.[13]

The VR display was found to be beneficial even for viewing static data sets. This is hardly surprising, since such data sets are often rendered for publication as shaded 3D images and give the audience a better understanding of the surface shape.

All of the data about the surface that has been scanned is already available to the scientist in a simple pseudo-color view from above. In this simple data presentation, the scientist can also measure any feature of the data to exacting precision using standard techniques such as cross sections and statistical algorithms. The benefit of visualization comes from getting multiple naturally controlled views of the data that may reveal unexpected insights. Some of the users had examined one data set using pseudo-color images and cross sections for months, yet discovered an important feature of the data (graphite sheets coming out of the surface) within seconds of viewing a real-time fly-over of the data set. These sheets were visible in only a few frames of the fly-over, when the lighting and eye point were in just the right position to highlight them.[12] Each frame in a real-time display of the surface can be considered as a new filter applied to the data set, with the user in control of the filter parameters (viewpoint, lighting direction) through natural motions of head and hand. People are adept at understanding the structure of 3D surfaces this way, having learned this skill over a lifetime.

Sometimes, though, viewing the surface in a two-dimensional display might be better. For flat surfaces with small features, a pseudo-color view is superior to the shaded 3D view for two reasons: First, the pseudo-coloring devotes the entire intensity range to depth and second, this method obscures small fluctuations caused by noise in the image. For features that are significant only for their height difference from the rest of the image, the pseudo-color image devotes its entire range of intensities to showing this difference. This is equivalent to drawing the surface from above using only ambient lighting with color based on height. Any 3D shading of the image uses some of this range to accommodate the diffuse and specular components at the expense of the ambient component.

This shift from ambient to diffuse/specular is a shift from displaying height to displaying slope (angle is what determines the brightness of the diffuse and specular components). This is fine for a noise-free image, but real-world images contain noise. For AFM images, a flat surface has the highest percentage of noise as a fraction of feature size. The noise causes

fluctuations in illumination of the same magnitude as those caused by features, sometimes completely obscuring them.

In summary, it was found that small features on flat surfaces are better seen using standard pseudo-color display (and are sometimes imperceptible in a 3D display). Small features on surfaces with other height variations are better brought out using specular highlighting of a 3D surface (and are often imperceptible in a 2D display). Both observations have been confirmed when making patterns on photo-resist and when etching lines into thin metal films. The nanoManipulator provides both the 2D and 3D views simultaneously; each updated live as the experiment progresses.

Haptics: a sense of touch The force feedback component of the nanoManipulator system has always been exciting to the scientists on the team, as they can feel the surface they are investigating. However, it is during modification that force feedback has been found to be most useful, allowing finer control and enabling whole new types of experiments. Force feedback has proved essential to finding the right spot to start a modification, finding the path along which to modify, and providing a finer touch than would be permitted by the standard scan–modify–scan experiment cycle.

Due to drift and hysteresis in the piezoceramic positioners used by AFMs to move the tip, the actual tip position may depend on environmental conditions and the history of the experiment. Therefore, the location of the tip relative to the sample might change over time. This makes it difficult to plan modifications accurately based only on an image that is reconstructed from scanned data. Force feedback, on the other hand, allows the user to locate objects and features on the surface by feel while the tip is making the modification. Surface features marking a desired region can be located without relying only on visual feedback from the previous scan. For instance, force feedback has been used to position the tip directly over an adenovirus particle, followed by an increase in the normal force to dimple the particle directly in its center. In the experiment described in Figure 4, the force feedback was also used to locate an adenovirus despite large drift and translocate it subsequently. Furthermore, this feature allowed the tip to be placed between two touching carbon filaments in order to tease them apart.[13]

At times, the need arises to perform multiple manipulations on a sample without having the possibility to scan the sample after each manipulation. In such a scenario, the location of the sample is no longer known after the first manipulation (as it is not reimaged). However, with the present system, the subsequent manipulations can still be carried out since the location of the sample can be identified using the force feedback feature.

"Haptic imaging" On some surfaces (i.e., graphite), carbon nanotubes are weakly attached to the substrate, and they are moved by the tip during scanning—even when using tapping mode imaging. In this case it is difficult to image the tube. By using touch mode only and switching between imaging and modification force, the scientists moved and reoriented one carbon nanotube and positioned it alongside another tube. Once settled against the other tube, it was stable and it could, again, be imaged by the scanning tip. Force feedback and slow, precise hand motion ("haptic imaging") made it possible to find the tube at intermediate points when it could not be seen with a regular scan. A description of haptic feedback research within the resource can be found in Brooks et al.[14]

SCIENTIFIC INVESTIGATIONS USING THE NANOMANIPULATOR

The scientific efforts undertaken by the nanoManipulator team are focused on biological and materials sciences samples. The most significant, recent results found by the team are outlined below. The investigated biological samples were fibrin, DNA,[8] tobacco mosaic virus,[15] and adenovirus, and the materials science sample comprised thin metal films, gold colloid particles, and carbon nanotubes or a combination of them.[16–18]

Manipulation of Biological Samples

The mechanical and interfacial properties of biological systems are important in understanding their biological function, structural stability and transport. The AFM holds promise of being a powerful tool in investigating these properties as it offers unique capabilities for the structural and mechanical study of biological systems. By virtue of the precise control of the position of the sharp tip and the quantitative measurement of tip–sample forces, AFM can combine nanometer-scale imaging with the determination of mechanical properties. For example, AFM has been used for the direct measurement of the adhesion force between the ligand–receptor pair biotin and avidin,[19] the forces between complementary strands of DNA,[20] the viscoelasticity of cell membranes,[21] and the rigidity modulus of bone.[22]

Manipulation of fibrin fibers Fibrin fibers are the major structural component of blood clots. Determining the strength and mechanical properties of blood clots will provide new insights into the wound-healing process and will advance our understanding of heart attacks and strokes. In the study described here, the rupture force and mechanical properties of individual fibrin fibers are being measured (Figure 2). Images of typical manipulations of these fibers are shown in Figure 2a and b and in Figure 2d and e. Figure 2a and d show the fibers before the manipulation, during which a lateral force was applied to the fiber until it ruptured. Figure 2b and e depict the fiber after the manipulation and Figure 2c and f show the respective lateral force traces that were recorded during the manipulations. The lateral force traces show two steps and two peaks. The two steps are due to a reversal in the direction of tip travel (i.e., from left to right and then from right to left) and correspond to the friction between the substrate and the tip. They are not of interest in the current study. However, the two peaks in the lateral force traces, which were a common feature in the measurements of all fibers (~30 fibers were manipulated) contain information about the mechanical properties of fibrin. By comparing the images with the lateral force traces it can be deduced that the first peak occurs when the tip contacts the fiber and partially detaches it from the surface. As the tip continues its travel, the fiber becomes taut again and is being stretched out. At this point, the force again increases rapidly and until the rupture point is reached. From such curves the rupture force of human fibrin was determined. Furthermore, the manipulation depicted in Figure 2d and e suggests that the deformation in the fibrin fiber is—at least partially—elastic. The fiber was initially bent further than the bend that is seen in

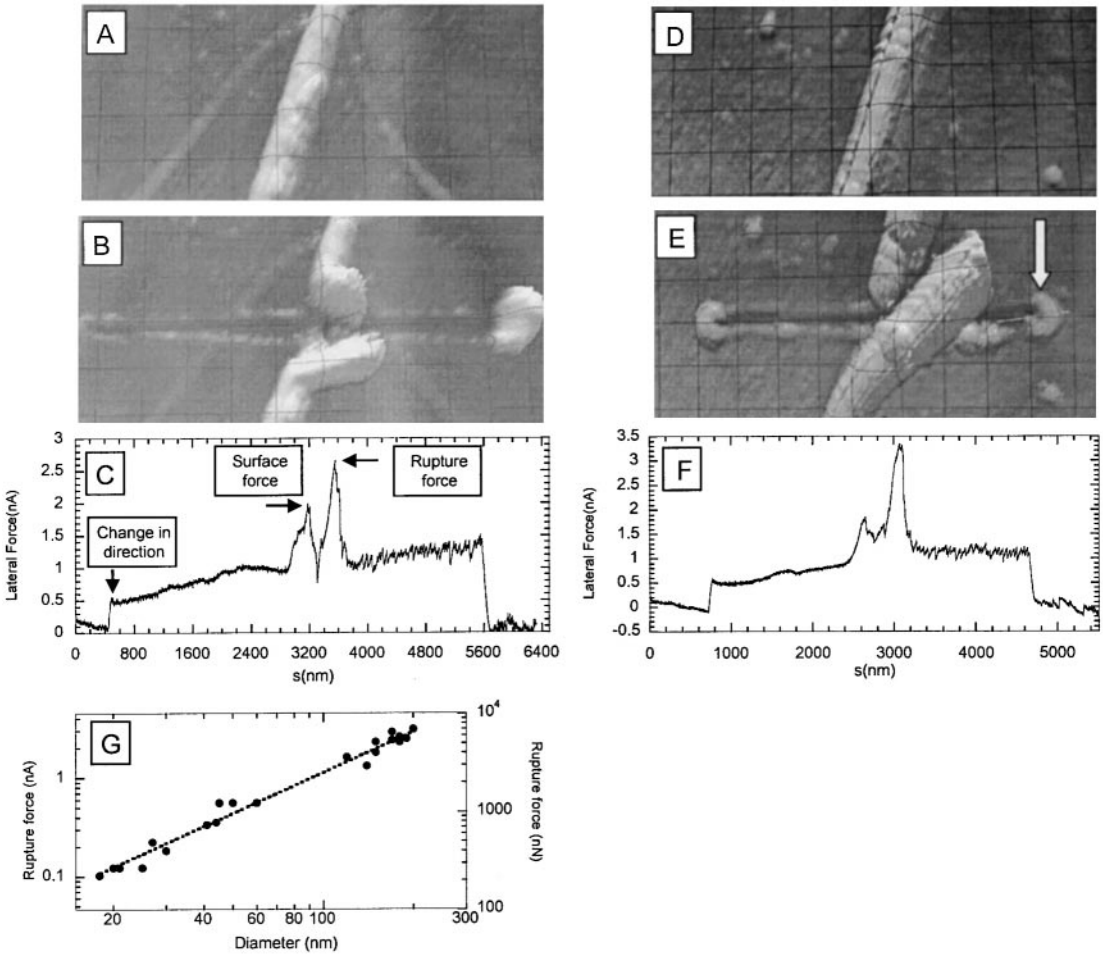

Figure 2. Manipulation of fibrin. (a–c) Manipulation of fibrin fiber 1 (diameter, 150 nm). Fibrin before (a) and after (b) manipulation. (c) Lateral force trace for manipulation of fiber 1. (d and e) Manipulation of fibrin fiber 2 (diameter, 180 nm). Fibrin before (d) and after (e) manipulation. The fiber moved back toward its original location, indicative of an elastic deformation. This elastic behavior has been observed for several fibers. (f) Lateral force trace for manipulation of fiber 2. (g) Rupture force versus diameter of fiber (logarithmic scale). The deduced exponent is about 1.4.

Figure 2e. In fact, it had been bent all the way to the end of the scratch that is left by the tip in the surface (Figure 2e, arrow). The fiber then moved back toward its straight configuration, because of a restoring force. Such behavior indicates that the bending of the fiber was elastic (possibly in addition to a permanent plastic deformation). The dependence of the rupture force on the diameter of the fiber (using logarithmic axis) is shown in Figure 2g. The rupture force increases proportional to $R^{1.4}$.

Manipulation of tobacco mosaic virus This study concerns tobacco mosaic virus (TMV), which, beyond its historical interest in biology, has served as a model system for the self-assembly process[23] and for statistical mechanical studies of the diffusion of rod-shaped particles.[24] We expect that the study of the elastic properties, mechanical stability, and surface binding of TMV and other viruses will shed light on the thermodynamics of self-assembly, their transport properties on surfaces, and the uncoating process in cells. In addition, the simple, rigid, rodlike structure of TMV makes it attractive as a model system for studies of the manipulation of delicate macromolecular systems. When manipulating an elongated object such as a TMV on a substrate, the resultant deformation is a function of the object's mechanical rigidity and the object–substrate friction.[15]

An example of a manipulation that gives insight into the mechanical properties of TMV is shown in Figure 3. The TMV particle has been adsorbed onto a graphite substrate and the experiment was done under ambient conditions. This particle, which is 232 nm long and 18 nm in diameter (a single virus capsid), is pushed near the center in a direction perpendicular to its long axis. The particle is rotated in several steps through an angle of almost 90 degrees while maintaining a relatively straight shape. In this case the particle exhibits rigid rodlike behavior, indicating that its mechanical rigidity is comparable to the substrate frictional forces. A simple mechanical model that incorporates the distributed friction and the mechanical rigidity was used to make an estimate of the Young's modulus of the TMV. It was found to be 1 GPa. As a frame of reference, steel has a Young's modulus of about 200 GPa, while nylon has a modulus of about 2 MPa. Our estimate is consistent with reported values for the Young's modulus of biological fiber structures.[25–28]

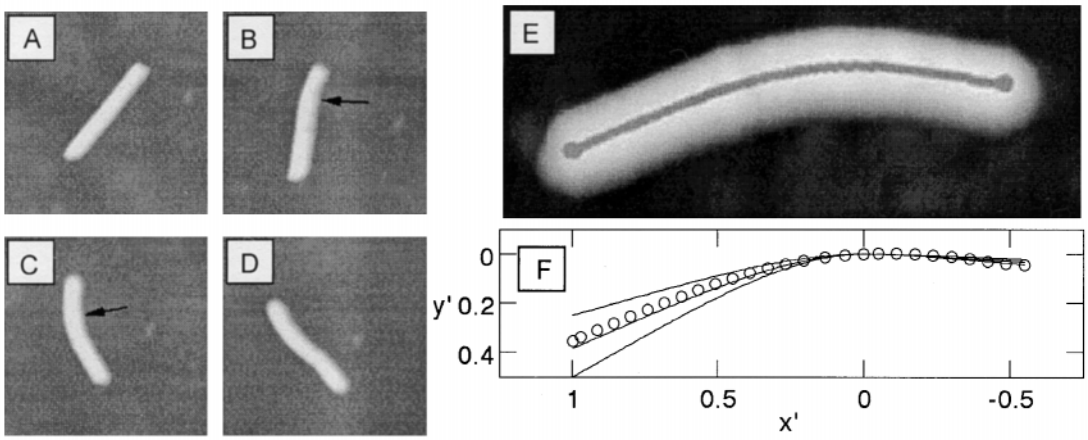

Figure 3. Rotation and bending of TMV particle (232 nm long, 18 nm in diameter) on graphite. In (a), the particle sits in its original adsorbed orientation. The AFM tip is then used to rotate the particle in successive pushes (b–d). The tip is moved in a counterclockwise orientation and makes contact with the virus as indicated by the arrows. (e) Ridge of manipulated TMV from (c). The figure has been rotated to match the orientation of plot. (f) Beam equation and fit. The beam-bending equation is simply plotted for three values corresponding to three values of Young's modulus. The middle curve is the best fit of the beam equation to the ridge data, corresponding to a Young's modulus of 1 GPa. Since the virus was not pushed in the middle, the beam equation is modified appropriately for the different lengths on either side of the point of tip contact.

Manipulation of adenoviruses on a silicon surface Knowing the interaction force between viruses and various materials is of great interest in virology, yet little is known about the behavior or motion of viruses on surfaces. For instance, outside of the host viruses may remain functional on surfaces for some time, and as they adhere to these surfaces, they may possibly translate on them. Furthermore, it is important to understand whether their structural integrity may be affected by the interaction between the protein capsid and the surface they land on. Moreover, after first attaching to a potential host cell, the viruses must translate over the cell surface to find the binding site where it can enter the cell. Accordingly, our understanding of the infection cycle could be advanced if it were possible to measure the forces required to translate a virus particle across surfaces. As a first step toward this goal, the force to push an adenovirus in an aqueous environment over a clean silicon surface was determined in this study.

Adenovirus was deposited onto silicon and imaged in water by the magnetic tapping mode. The virus in the center of Figure 4a is translated to the right in two separate pushes; the result of each push is shown in Figure 4b and 4c. The first attempt to translate the virus failed, the tip missed the virus due to drift of the sample position. In the next attempt—unlike the first one—the virus was located by haptic force feedback before switching

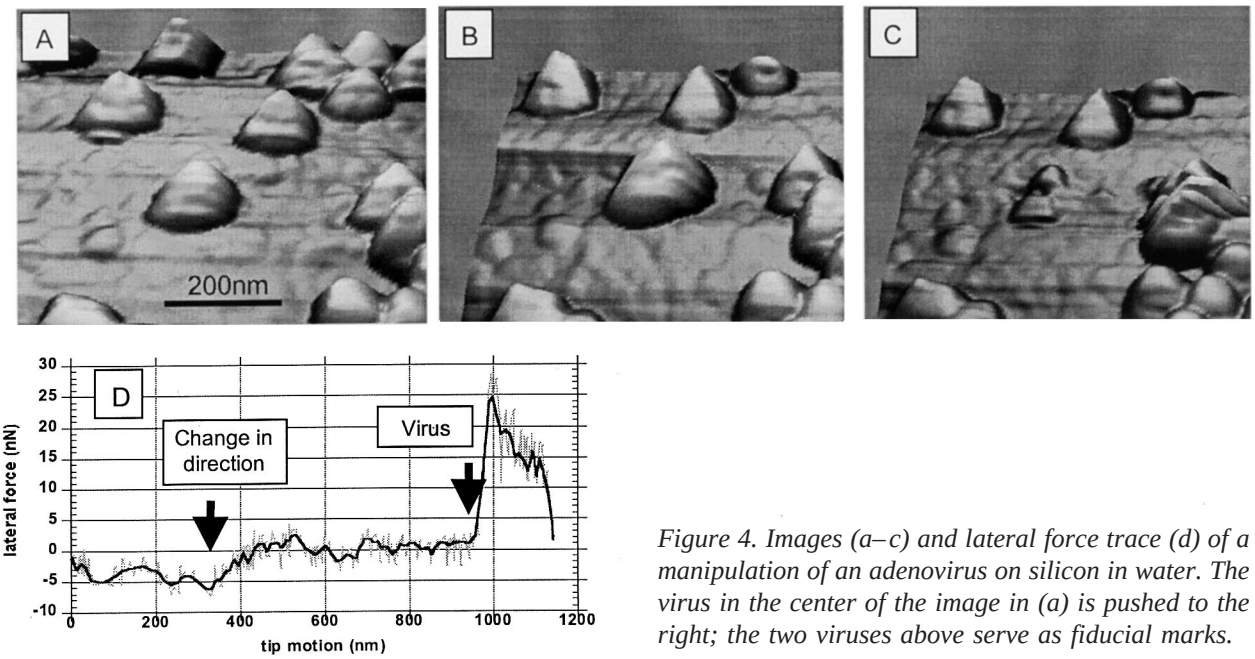

Figure 4. Images (a–c) and lateral force trace (d) of a manipulation of an adenovirus on silicon in water. The virus in the center of the image in (a) is pushed to the right; the two viruses above serve as fiducial marks.

to contact mode for the application of the lateral force. A plot of the lateral force versus the motion of the tip is shown in Figure 4d. The force trace of the tip pushing the virus appears to have two regimes: an initial high adhesive regime followed by one in which a lower force, or possibly a decreasing force, is needed to continue translating the virus. A force of approximately 25 nN is needed to start the virus moving, and a force of 12 nN is then required to maintain the motion. There may be several explanations for this behavior. First, there could be the equivalent of the macroscopic static friction that must be overcome before the lower force due to sliding friction is seen. Second, the virus could be sliding off the side of the tip, so that less force is actually being applied to the virus as it is no longer fully translated. Finally, there could be a layer of salts, such as cesium chloride from the storage buffer, between the virus and the substrate. Pushing the virus off this layer and onto clean substrate could require a higher lateral force than that required for translating it over the surface alone. In the final image there can be seen some residue left behind after the virus has been moved, and so this last interpretation seems a likely explanation.

Manipulation of DNA The genetic information of all living organisms is stored in their DNA, making DNA one of the most important molecules in the biological sciences. Knowing the tensile strength and other mechanical properties of DNA is crucial to gaining a better understanding of many cellular processes. DNA, being the molecule that carries the genetic information, is continuously manipulated and pulled on by the cellular machinery during transcription, replication, and the regulation of these processes. DNA also undergoes mechanical strains when it is wrapped around proteins and histones, when it is packed into virus capsids, or when it is folded into chromatin and chromosomes. Furthermore, DNA is subjected to large tensile forces during anaphase in the cell division cycle.[29] In the past, some of the elastic properties of DNA, such as Young's modulus and the persistence length, have been measured indirectly.[30–35] DNA has also been dissected with the tip of an SFM, but no mechanical parameters have been measured in these experiments.[36–38]

In the present work, DNA was manipulated with the nanoManipulator and the rupture force of DNA was measured directly. Figure 5 shows a typical image of a controlled manipulation of a 1100-bp (372-nm)-long DNA fragment. In Figure 5a the fragment is seen before the manipulation. The dark arrow indicates the path of the tip during manipulation; the tip was first moved from left to right and then from right to left over the molecule. The normal force, which was kept constant throughout the manipulation, was approximately 25 nN. The fragment after the manipulation is depicted in Figure 5b. It can be clearly seen that the tip severed the DNA at the intended point of intersection. From the width of the DNA a tip diameter of about 15 nm is estimated, which corresponds well to the width of the gap that was cut into the DNA fragment. From these experiments, it was determined that a force of about 500 pN is required to rupture both strands of the DNA molecule (Figure 5c). In these experiments the rupture force of DNA was determined *directly* for the first time. The obtained value agrees with the value that has been estimated from another, more indirect experiment.[35]

Carbon Nanotubes

Mechanical properties of carbon nanotubes Carbon nanotubes (CNTs) are simply graphite tubes of nanometer scale. The graphite sheet is wrapped seamlessly into a tube shape and sometimes many such tubes are arranged in a coaxial structure known as a multiwall carbon nanotube. The carbon–carbon bond is the strongest bond in nature and is the reason why diamond is the hardest material known. This bond in the carbon nanotube makes it a material with remarkable mechanical properties. It is both stiff (requires large force per unit deformation) and flexible (able to withstand large deformation without damage). We have used the NanoManipulator to study the mechanical properties of CNTs by bending and pushing them on surfaces.

In Figure 6, an ~800-nm-long tube with a radius of ~6.8 nm was bent repeatedly to large strain with no permanent distortion of the tube topography. The sequence of figures on the left of Figure 6 illustrates the entire manipulation process of the tube-bending experiment. The sequence has been included to demonstrate clearly the number of manipulations that were performed in the experiment. Each increment in the gradually increasing bending is imaged. No relaxation was observed during the entire sequence. Note that despite the bending forward, back, and then forward again, the tube in the final image appears to be undamaged (Figure 6).

The height of the tube in Figure 6 always remains within the bounds of a flattened tube, even after being bent through the sequence of curvature radii: +20 nm, −20 nm, +40 nm, where positive curvature has been assigned to Figure 6b. The maximum local strain in this tube can be estimated from the ratio of the tube radius to the radius of curvature $\epsilon = r_0/r_\kappa \approx 16\%$ on the outside tube surface, with a corresponding compressive

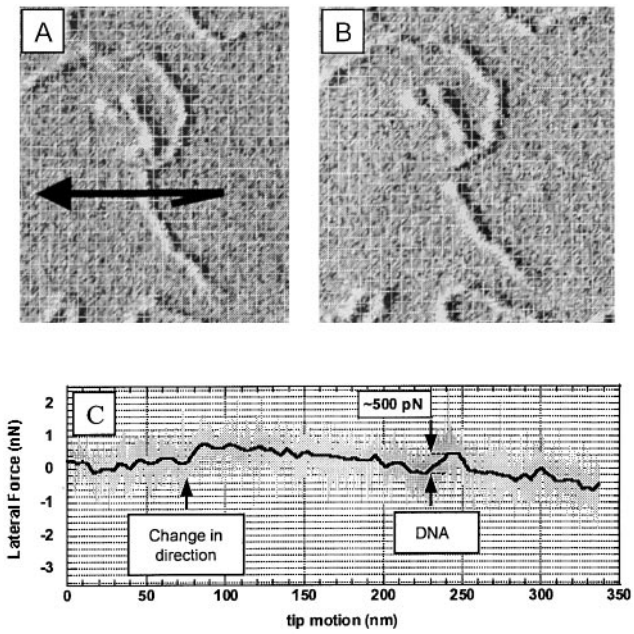

Figure 5. DNA fragment before (a) and after (b) it has been manipulated. The dark arrow indicates the path of the tip. A gap, about 15 nm wide, is seen where the tip intersected the DNA. Grid, 10 nm. (c) Plot of the lateral force versus the distance traveled by the tip.

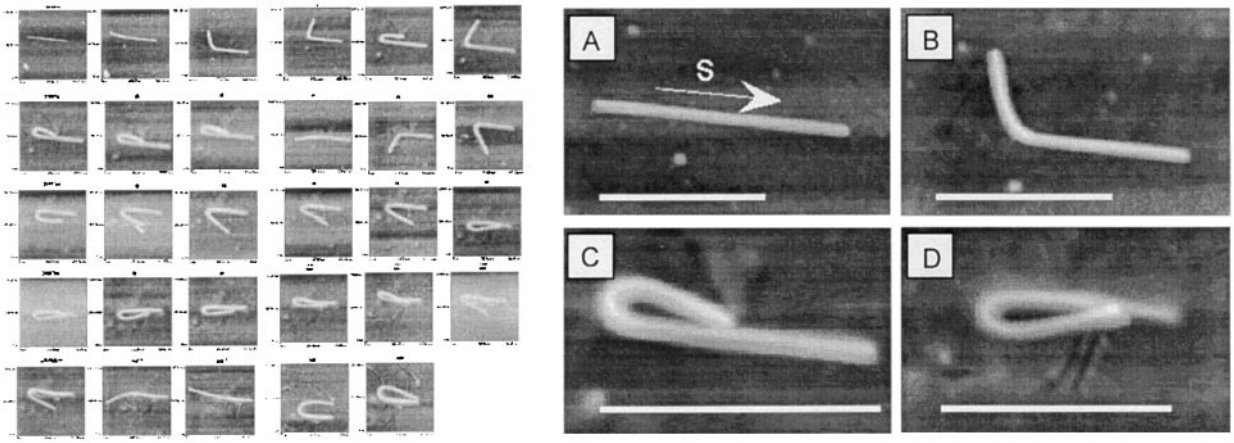

Figure 6. Carbon nanotube in highly strained configuration. The sequence on the left depicts the entire AFM manipulation process. The white scale bars at the bottoms of (a)–(d) represent a length of 500 nm. (a) The original adsorbed shape of the tube is 10.5 nm in diameter and 850 nm in length. The tube is bent in steps, first upward (b) and then back onto itself (c). The curvature is 0.045/nm (radius of curvature, ~20 nm), which indicates the strain along the inside and outside of tube bend is ~16%. (d) The tube is then bent back the other way onto itself to a final curvature similar to that in (c).

strain on the inner surface. The apparent lack of catastrophic damage of the tube under such large strains is remarkable. It can be speculated that the strain has been accommodated in one of two ways: First, it has been proposed that multiwall CNTs contain a significant concentration of defects. It might be that defects in this tube are arranged in an incoherent fashion such that they separate under tensile stress, and slide over each other reversibly under compressive stress. Second, strain might be accommodated within a severely distorted, but otherwise connected, graphene sheet. MD simulations of single-walled tubes under tensile strain have shown, under certain conditions, breaking strains as large as 30%.[39]

Friction In this experiment multiwall CNTs were manipulated on surfaces to investigate the frictional forces involved in the process. A measure of the force required to initiate and maintain motion gives insight into the interfacial energy and contact mechanics between a particle and substrate. In a practical context, these properties are relevant in assessing the potential use of CNTs as lubricants, as reinforcements in composite materials, and as molecular-scale mechanical mechanisms. In a fundamental sense, these experiments begin to answer basic questions about the motion of nanometer-scale objects. Do they roll or slide and why? What is the physics behind the resistance to sliding or rolling? Wearless friction at the nanometer scale is not yet well understood.

A large multiwall CNT on a graphite substrate is selected for manipulation as pictured in Figure 7. One end of this tube has a pronounced "bump." The tube is pushed from the side (perpendicular to its axis) and the tube rolls as evident by the reorientation of the bump. But when pushed past the point where the bump rolls over and contacts the surface, rolling stops and the tube slides. The topographical evidence shows that the bump remains on the same side with the same orientation while the tube is pushed further in the same direction. When the tube is pushed the other way side-on, the tube rolls over the other way until it is stopped by the bump. A schematic is shown in the inset. The lateral force data signals are consistent with this interpretation (Figure 7a–c). The diameter of the cylindrical portion of the tube is 39 nm, giving it a circumference of 123 nm. The lateral force signal abruptly changes at 75 nm after pushing begins. This is the case for pushing in both directions (rolling both ways). Assuming the tube is rolling on a cylindrical contact region 39 nm in diameter, it rolls through 220 degrees before sliding begins.

An interesting aspect of this example is the transition from rolling to sliding. The change in the lateral force at this point is dramatic and counterintuitive. Why is the sliding force lower than the peaks in the rolling force? This can be explained with an adhesive model for the rolling. As the asymmetric tube rolls, it goes through a series of pull-off events as the contacting regions at different points along the tube's circumference release from the surface. If the tube is more polygonal than round, different "faces" of the tube will have varying adhesive strengths depending on the different contact area of each point along the tube. The pull-off force for a contact zone can be much higher than the force required to slide it. This model relies on the tube's asymmetry and is hard to apply to the case of a perfectly cylindrical tube. The harder question to answer is why the tube prefers rolling for the initial portion of the motion when the sliding force is lower. This is unclear. Assuming that there are three thresholds involved—the force required to roll the tube, the force required to initiate motion (static friction), and the force required to maintain motion (kinetic sliding friction)—it can be argued that the observed behavior follows. As the tube rolls, it sticks and slips but at no point is the tube sliding. If the threshold force of rolling is lower than the force required to initiate sliding, then the tube doesn't slide and continues to roll. But if at some point it does begin sliding and the force required to maintain sliding motion is lower than rolling force, then the tube will slide rather than roll. If the resistance to rolling is due to adhesion, this argument suggests that we should expect larger lateral force for rolling than for sliding. Why the rolling is preferred for the initial portion of the motion is still unclear, however. More detailed discussion of our studies of rolling friction can be found elsewhere.[17,40]

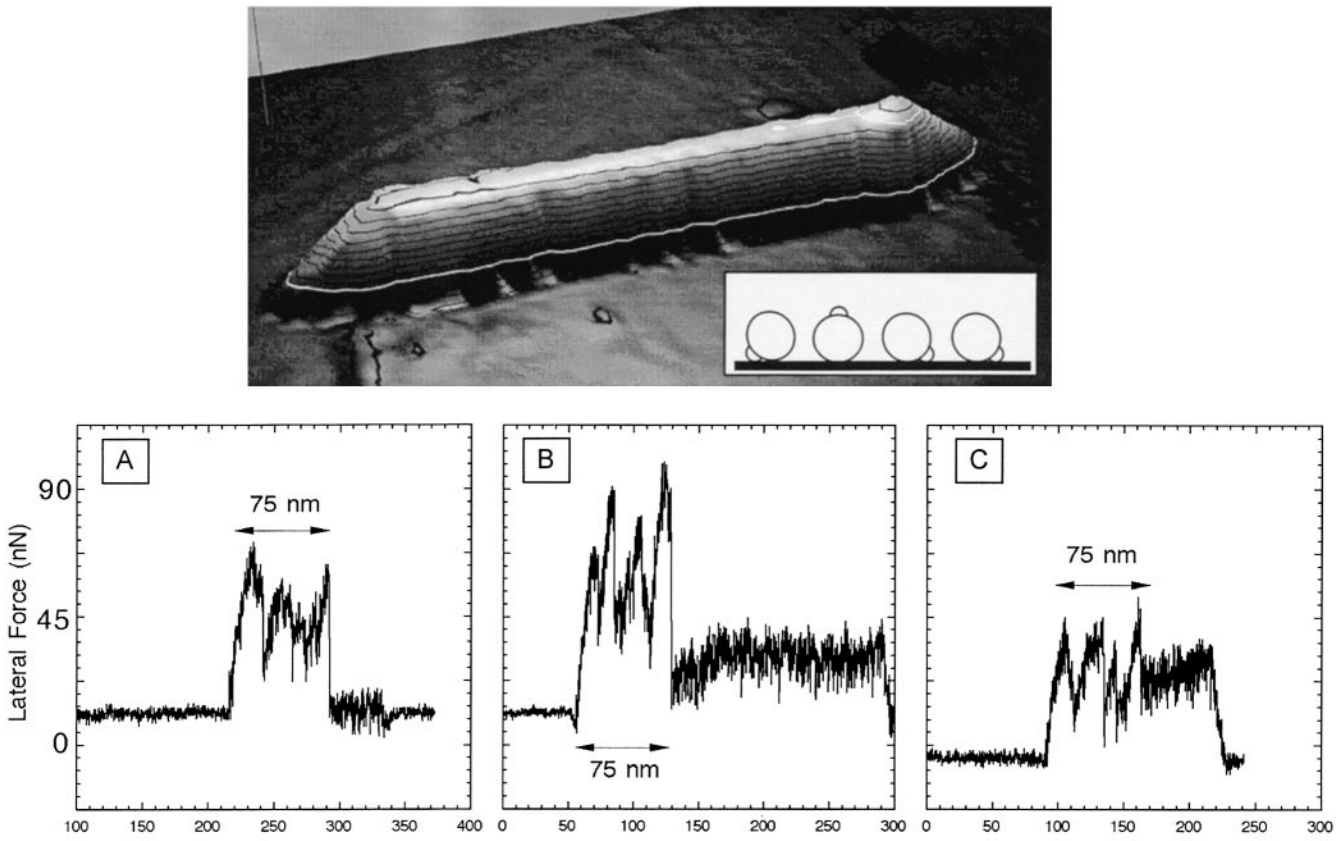

Figure 7. Tube (~500 nm) with a "bump." On the far right side of the tube a feature projects out of the cylindrical body of the tube. Inset: *End-on-view of the tube with the bump, showing a model of the roll-to-slide transition. The topographical images indicate that the tube rolls over until the bump contacts the surface, at which point the tube slides. The tube is able to roll through ~220 degrees and then begins sliding when the bump contacts on the other side. (a–c) Lateral force during the roll-to-slide transition. (a) and (c) are for forward rolling and (b) is for reverse rolling. In all three cases ~75 nm of slip stick signal associated with rolling precedes a flat region associated with the sliding. In each case the tube was rolled from bump contact on one side to bump contact on the other side, as indicated the topographical data. This corresponds to a 220-degree roll.*

AFM lithography and electromechanical studies on carbon nanotubes In addition to the interest in the mechanical properties of carbon nanotubes, there has been considerable theoretical and experimental effort to understand the electrical properties of these nanostructures. Theoretical studies made soon after their discovery,[41] and more recent experimental work,[42,43] suggest that nanotubes have electronic band structure ranging from metallic to moderate bandgap (~1 eV) semiconductors. Carbon nanotubes may also be ideal structures to study the fundamental properties of one-dimensional (1-D) systems. As electrons are confined in one or more dimensions by interfaces or device edges, behavior drastically different from that in bulk material is observed. While 2-D and 0-D systems have been studied experimentally, it has been difficult to manufacture 1-D structures clean enough to observe the predicted behavior. Because of their small diameter and unique geometry it is possible that carbon nanotubes may be a testing ground for this behavior.

A major difficulty in studying the properties of carbon nanotubes is in making good electrical contact to such small objects placed in arbitrary locations on a substrate. We have combined standard photolithography and AFM lithography based on the NanoManipulator to tackle this problem. Nanotubes are dispersed on an oxidized silicon wafer, and coated with a thin (~100 nm) metal film. After photolithography defines large-scale (5 μm) features, the sample is imaged to identify the location of nanotubes with respect to the large features. The sample is then coated with a thin layer of soft polymer, and the nanoManipulator is used to clear a path in the polymer one to three hundred nanometers wide. With the help of the haptic feedback, this can be done on top of a nanotube, with almost perfect registry to any topographical feature. The sample is then placed in a chemical etchant that dissolves the metal only where the polymer was removed, leaving two separated metal leads, connected only by the nanotube. Using this technique, resistance measurements of several multiwall nanotubes have been carried out. More advanced devices with feature sizes as small as 250 nm, and registered to a carbon nanotube within ten nanometers have also been produced. Figure 8a shows an example of such a CNT device made using the nanoManipulator as a lithography tool.

An AFM tip, as seen in the preceding discussion of manipulations, can be extremely useful to interact mechanically and hence electrically with a sample in a highly localized area. An interesting question, and the subject of significant theoretical work, is how mechanical strain of a nanotube affects its electrical behavior.[44] Pursuing these ideas, the nanoManipulator

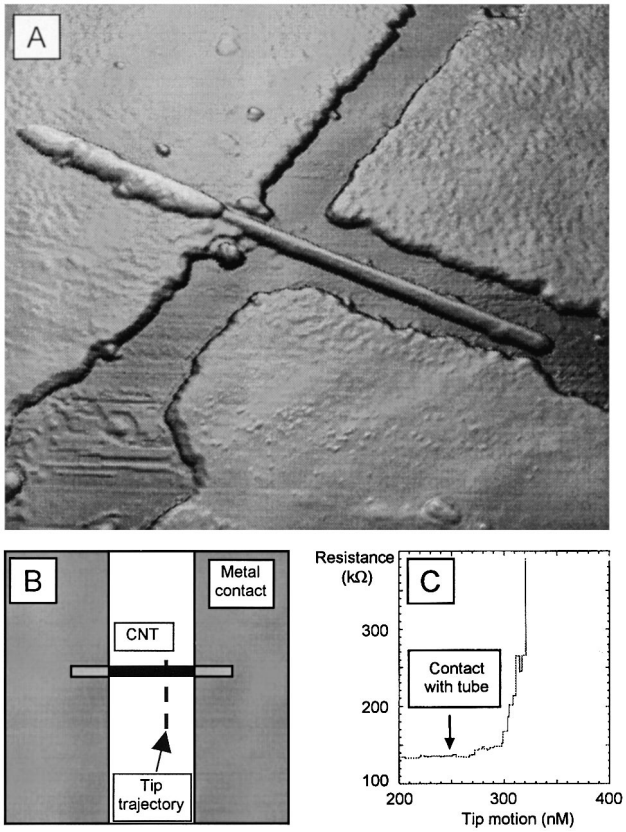

Figure 8. (a) A prototype nanotube actuator built with nanoManipulator lithography. The narrowest gap is 250 nm. The tube is 30 nm in diameter. (b) Experimental setup to measure resistance versus strain. The AFM tip is pushed through the CNT, while the resistance is being measured. (c) Plot of resistance versus tip position as tip is pushed through the nanotube. Notice that the change in resistance occurs over a 50-nm span.

was used to apply a mechanical strain to a carbon nanotube while measuring its resistance in situ (Figure 8b and c). First, in a control experiment, it was found that running the tip over the sample with moderate force showed no measurable effect. However, when the tip pushed laterally through the tube, causing the tube to bend, the resistance was observed to change gradually from 130 to 250 kW. Further pushing on the tube caused the resistance to become immeasurably large ($>$ 10 000 kW), and subsequent imaging of the sample showed the nanotube was broken into two separate pieces. We were then able to push the two pieces into contact with each other, again closing the circuit. The resistance of the junction could be tuned to numerous stable values between 200 and 500 kW.[45] Further studies on the nature of this junction are underway.

CONCLUDING REMARKS

This article describes the nanoManipulator system and the scientific experiments that have been carried out using this system. It is a part of an NIH National Research Resource and as such is available for use by outside visitors for their experiments. Investigators interested in using the system can obtain more information at *http://www.cs.unc.edu/Research/nano/doc/biovisit.html.*

ACKNOWLEDGMENTS

This work was supported by the National Institutes of Health (National Center for Research Resources; Grant NIH NCRR 5-P41-RR02170), the National Science Foundation (Grants NSF HPCC ASC-9527192, NSF ARI DMR-9512431, and NSF CISE CDA-9504293), the ORN MURI Research Initiative, and the ARO DURIP Instrumentation Program. Equipment was provided by Topometrix, Inc., Silicon Graphics, Inc., and Intel, Inc.

REFERENCES

1 Binnig, G., Quate, C.F., and Gerber, C.H. Atomic force microscope. *Phys. Rev. Lett.* 1986, **56,** 930–933
2 Guthold, M., Bezanilla, M., Erie, D.A., Jenkins, B., Hansma, H.G., and Bustamante, C. Following the assembly of RNA polymerase–DNA complexes in aqueous solutions with the scanning force microscope. *Proc. Natl. Acad. Sci. U.S.A.* 1994, **91,** 12927–12931
3 Zhong, Q., Inniss, D., Kjoller, K., and Elings, V.B. Fractured polymer silica fiber surface studied by tapping mode atomic force microscopy. *Surf. Sci.* 1993, **290,** L688–L692
4 Guthold, M., Zhu, X., Rivetti, C., Yang, G., Thomson, N.H., Kasas, S., Hansma, H.G., Smith, B., Hansma, P.K., and Bustamante, C. Direct observation of one-dimensional diffusion and transcription by Escherichia coli RNA polymerase. *Biophys. J.* 1999, **77,** 2284–2294
5 Ratcliff, G.C., Erie, D.A., and Superfine, R. Photothermal oscillation for oscillating mode atomic force microscopy in solution. *Appl. Phys. Lett.* 1998, **72,** 1911–1913
6 Han, W., Lindsay, S.M., and Jing, T. A magnetically driven oscillating probe microscope for operation in liquids. *Appl. Phys. Lett.* 1996, **69,** 4111–4113
7 Hiller, A.C., and Bard, A.J. AC-mode atomic force microscope imaging in air and solutions with a thermally driven bimetallic cantilever probe. *Rev. Sci. Instrum.* 1997, **68,** 2082–2090
8 Guthold, M., Matthews, G., Negishi, A., Taylor, R.M., Erie, D., Brooks, F.P., and Superfine, R. Quantitative manipulation of DNA and viruses with the nanoManipulator scanning force microscope. *Surf. Interf. Anal.* 1999, **27,** 437–443
9 Stowe, T.D., Yasumura, K., Kenny, T.W., Botkin, D., Wago, K., and Rugar, D. Attonewton force detection using ultrathin silicon cantilevers. *Appl. Phys. Lett.* 1997, **71,** 288–290
10 Cleveland, J.P., Manne, S., Bocek, D., and Hansma, P.K. A nondestructive method for determining the spring constant of cantilevers for scanning force microscopy. *Rev. Sci. Instrum.* 1993, **64,** 403–405
11 Finch, M., Chi, V.L., Taylor, R.M., Falvo, M., Washburn, S., and Superfine, R. Surface modification tools in a virtual environment interface to a scanning probe microscope. In: *Proceedings of the ACM Symposium on Interactive 3D Graphics, Monterey, CA.* Association for Computing Machinery, SIGGRAPH, New York, 1995, pp. 13–18
12 Taylor, R.M., Robinett, W., Chi, V.L., Brooks, F.P., Wright, W.V, Williams, S., and Snyder, E.J. The nanoManipulator: A virtual-reality interface for a scan-

ning tunneling microscope. In: *SIGGRAPH '93, Anaheim, CA.* ACM SIGGRAPH, New York, 1993, pp. 127–134
13 Taylor, R.M., Chen, J., Okimoto, S., Llopis-Artime, N., Chi, V.L., Brooks, F.P., Falvo, M., Paulson, S., Thiansathaporn, P., Glick, D., Washburn, S., and Superfine, R. Pearls found on the way to the ideal interface for scanned-probe microscopes. In: *Visualization '97*. IEEE Computer Society Press, Phoenix, AZ, 1997, pp. 467–470
14 Brooks, F.P., Ouh-Young, M., Batter, J.J., and Kilpatrick, P.J. Project GROPE—haptic displays for scientific visualization. In: *Computer Graphics: Proceedings of SIGGRAPH '90*, ACM-SIGGRAPH Vol. 24. Dallas, Texas, 1990, pp. 177–185
15 Falvo, M.R., Washburn, S., Superfine, R., Finch, M., Brooks, F.P., Chi, V., and Taylor, R.M. Manipulation of individual viruses: Friction and mechanical properties. *Biophys. J.* 1997, **72,** 1396–1403
16 Taylor, R.M., Williams, R.S., Chi, V.L., Bishop, G., Fletcher, J., Robinett, W., and Washburn, S. Nanowelding: Tip response during STM modification of Au surfaces. *Surf. Sci. Lett.* 1994, **306,** 534–538
17 Falvo, M.R., Taylor, R.M., Helser, A., Chi, V., Brooks, F.P., Washburn, S., and Superfine, R. Nanometre-scale rolling and sliding of carbon nanotubes. *Nature (London)* 1999, **397,** 236–239
18 Falvo, M.R., Clary, G.J., Taylor, R.M., Chi, V., Brooks, F.P., Washburn, S., and Superfine, R. Bending and buckling of carbon nanotubes under large strain. *Nature (London)* 1997, **389,** 582–584
19 Florin, E.-L., Moy, V.T., and Gaub, H.E. Adhesion forces between individual ligand–receptor pairs. *Science* 1994, **264,** 415–417
20 Lee, G.U., Chrisey, L.A., and Colton, R.J. Direct measurement of the forces between complementary strands of DNA. *Science* 1994, **266,** 771–773
21 Putman, C., van der Werf, K.O., de Grooth, B.G., van Hulst, N.F., and Greve, J. Viscoelasticity of living cells allows high resolution imaging by tapping mode atomic force microscopy. *Biophys. J.* 1994, **67,** 1749–1753
22 Tao, N.J., Lindsay, S.M., and Lees, S. Measuring the microelastic properties of biological material. *Biophys. J.* 1992, **63,** 1165–1169
23 Caspar, D.L.D., and Klug, A. Physical principles in the construction of regular viruses. *Cold Spring Harbor Symp. Quant. Biol.* **27,** 1–24
24 Grossman, P.D., and Soane, D.S. Orientation effects on the electrophoretic mobility of rod-shaped molecules in free solution. *Anal. Chem.* 1990, **62,** 1592–1596
25 Elbaum, M., Kuchnir-Fygenson, D., and Libchaber, A. Buckling microtubules in vesicles. *Phys. Rev. Lett.* 1996, **76,** 4078–4081
26 Sirenko, Y.M., Strocio, M.A., and Kim, K.W. Elastic vibrations of microtubules in a fluid. *Phys. Rev. E* 1996, **53,** 1003–1010
27 Gittes, F., Mickey, B., Nettleton, J., and Howard, J. Flexural rigidity of microtubules and actin filaments measured from thermal fluctuations in shape. *J. Cell Biol.* 1993, **120,** 923–934
28 Venier, P., Maggs, A.C., Carlier, M.-F., and Pantaloni, D. Analysis of microtubule rigidity using hydrodynamic flow and thermal fluctuations. *J. Biol. Chem* 1994, **269,** 13353–13360
29 Jannink, G., Duplantier, B., and Sikorav, J.-L. Forces on chromosomal DNA during anaphase. *Biophys. J.* 1996, **71,** 451–465
30 Rivetti, C., Guthold, M., and Bustamante, C. Scanning force microscopy of DNA deposited on mica: Equilibration *versus* kinetic trapping studied by polymer chain analysis. *J. Mol. Biol.* 1996, **264,** 919–932
31 Wang, M.D., Yin, H., Landick, R., Gelles, J., and Block, S.M. Stretching DNA with optical tweezers. *Biophys. J.* 1997, **72,** 1335–1346
32 Smith, S.B., Cui, Y., and Bustamante, C. Overstretching B-DNA: The elastic response of individual double-stranded and single-stranded DNA molecules. *Science* 1996, **271,** 795–799
33 Cluzel, P., Lebrun, A., Heller, C., Lavery, R., Viovy, J.-L., Chatenay, D., and Caron, F. DNA: An extensible molecule. *Science* 1996, **271,** 792–794
34 Hagerman, P.J. Flexibility of DNA. *Annu. Rev. Biophys. Biophys. Chem.* 1988, **17,** 265–286
35 Bensimon, D., Simon, A.J., Croquette, V., and Bensimon, A. Stretching DNA with a receding meniscus: Experiments and models. *Phys. Rev. Lett.* 1995, **74,** 4754–4757
36 Henderson, E. Imaging and nanodissection of individual supercoiled plasmids by atomic force microscopy. *Nucleic Acids Res.* 1992, **20,** 445–447
37 Hansma, H.G., Vesenka, J., Siegerist, C., Kelderman, G., Morrett, H., Sinsheimer, R.L., Elings, V., Bustamante, C., and Hansma, P.K. Reproducible imaging and dissection of plasmid DNA under liquid with the atomic force microscope. *Science* 1992, **256,** 1180–1184
38 Vesenka, J., Guthold, M., Tang, C.L., Keller, D., Delaine, E., and Bustamante, C. Substrate preparation for reliable imaging of DNA molecules with the scanning force microscope. *Ultramicroscopy* 1992, **42,** 1243–1249
39 Yakobson, B.I., Campbell, M.P., Brabec, C.J., and Bernholc, J. Tensile strength, atomistics of fracture, and C-chain unraveling in carbon nanotubes. *J. Comput.-Aided Mater. Design* 1997, **3,** 173
40 Falvo, M.R., Clary, G., Helser, A., Paulson, S., Taylor, R.M., Chi, V., Brooks, F.P., Washburn, S., and Superfine, R. Nanomanipulation experiments exploring frictional and mechanical properties of carbon nanotubes. *Microsc. Microanal.* 1999, **4,** 504–512
41 Dresselhaus, M.S., Dresselhaus, G., and Eklund, P.C. *Science of Fullerenes and Carbon Nanotubes.* Academic Press, San Diego, 1996
42 Odom, T.W., Huang, J.-L., Kim, P., and Lieber, C.M. Atomic structure and electronic properties of single walled carbon nanotubes. *Nature (London)* 1998, **391,** 62–64
43 Wildoer, J.W.G., Venema, L.C., Rinzler, A.G., Smalley, R.E., and Dekker, C. Electronic structure of atomically resolved carbon nanotubes. *Nature (London)* 1998, **391,** 59–62
44 Yang, L., Anantram, M.P., Han, J., and Lu, J.P. Band-gap change of carbon nanotubes: Effect of small uniaxial and torsional strain. *Phys. Rev. B* 1999, **60,** 13874–13878
45 Paulson, S., Falvo, M.R., Snider, N., Helser, A., Hudson, T., Seeger, A., Taylor, R.M., Superfine, R., and Washburn, S. In situ resistance measurements of strained carbon nanotubes. *Appl. Phys. Lett.* 1999, **75,** 2936–2938